THE ASTROPHYSICAL JOURNAL, 492:569–574, 1998 January 10

ORFEUS-I OBSERVATIONS OF MOLECULAR HYDROGEN IN THE GALACTIC DISK[1]

W. VAN DYKE DIXON, MARK HURWITZ, AND STUART BOWYER
Space Sciences Laboratory and Center for EUV Astrophysics, University of California, Berkeley, CA 94720-5030; vand@ssl.berkeley.edu
Received 1997 April 2; accepted 1997 August 21

ABSTRACT

We present measurements of interstellar H_2 absorption lines in the continuum spectra of seven early-type stars in the Galactic disk at distances between 1 and 4 kpc. Five of these stars provide lines of sight through the Sagittarius spiral arm. The spectra, obtained with the Berkeley EUV/FUV spectrometer on the ORFEUS telescope in 1993 September, have a resolution of 3000 and statistical signal-to-noise ratios between 20 and 80. We determine column densities for each observed rotational level and derive excitation temperatures and densities for the H_2 clouds along each line of sight. Our data continue the relationships among H_2 column density, fractional molecular abundance, and reddening apparent in *Copernicus* observations of nearby stars, indicating a common mechanism for H_2 production. Estimates of cloud temperatures and densities are consistent with those derived from *Copernicus* data. The molecular fraction f is nearly constant over a wide range of distances and mean reddenings, consistent with a model in which a significant fraction of the neutral ISM is associated with H_2-bearing molecular clouds, even along low-density lines of sight.

Subject headings: Galaxy: structure — ISM: abundances — ISM: molecules — ultraviolet: ISM

1. INTRODUCTION

The hydrogen molecule (H_2) plays a central role in a variety of processes that significantly influence the chemical and physical state of the interstellar medium (ISM). From observations by *Copernicus* and other spacecraft-borne observatories, a picture has emerged in which the bulk of interstellar H_2 lies in clouds with densities between ~ 10 and a few thousand cm^{-3}, diameters less than a few tens of parsecs, and column densities $\gtrsim 10^{20}$ cm^{-2}, which allow the rapid formation of H_2 on dust grains and provide self-shielding against dissociating photons (Wilson & Walmsley 1989). In order to determine whether this model, developed from observations of relatively nearby stars ($d \lesssim 2$ kpc), holds at larger distances, we observed seven stars in the Galactic disk ($|z| < 300$ pc) at distances out to 3.9 kpc, using the Berkeley spectrometer on the ORFEUS telescope.

2. OBSERVATIONS AND DATA REDUCTION

The Berkeley EUV/FUV spectrometer, located at the prime focus of the 1 m ORFEUS telescope, flew aboard the space platform ASTRO-SPAS during the 1993 September mission of *Discovery*. The ORFEUS project and the ASTRO-SPAS platform are described in Grewing et al. (1991), while the design and performance of the Berkeley spectrometer are discussed in Hurwitz & Bowyer (1991, 1995) and Hurwitz et al. (1995).

With an effective area of about 4 cm^2 and a resolution $\lambda/\Delta\lambda = 3000$ over the wavelength range 390–1170 Å, the Berkeley spectrometer is ideally suited for absorption-line studies of bright, far-UV sources. Some two dozen early-type stars were observed on the ORFEUS-I mission; in this paper we discuss the seven with $|z| < 300$ pc. Table 1 lists the stars and their observational parameters. Also given are the total ORFEUS integration time and the statistical signal-to-noise ratio (S/N) in a 0.2 Å bin, averaged over the 1045–1060 Å band in the resulting spectrum. The procedures for data extraction, background subtraction, and wavelength and flux calibration are described in Hurwitz & Bowyer (1996). The flux calibration is based on in-flight observations of the hot white dwarf G191-B2B and is thought to be uncertain to less than 10% (Vennes & Fontaine 1992). A segment of the ORFEUS spectrum of HD 99890 is presented in Figure 1; the spectrum is rich in molecular hydrogen features and the atomic lines of H, N, Ar, and Fe.

We model the interstellar absorption features using an ISM line-fitting package written by M. Hurwitz and V. Saba. Given the column density, Doppler broadening parameter, and relative velocity of a given species, the program computes a Voigt profile for each line, convolves the lines with a Gaussian to the instrument resolution, and uses the result as a transmission function by which to scale the model continuum. Given these assumptions, the only free parameters in the fit are the continuum placement and the total column density of each absorbing species.

In principle, it is possible to derive the effective Doppler parameter directly from the ORFEUS data by measuring the equivalent widths of many absorption features from a given J'' level, sampling a range of oscillator strengths. In practice, line blending, continuum placement uncertainties, and the limited dynamic range of the accessible oscillator strengths make such analyses difficult. The resulting constraints on the effective Doppler parameters (typically 5–8 km s^{-1}) almost certainly reflect velocity-component structure rather than line broadening in a single cloud. Instead, for the four lines of sight listed in Table 2, we take the Doppler parameters, relative velocities, and relative column densities of the principal absorption components from the literature. For the remaining lines of sight, we assume a single absorption component with a Doppler parameter $b = 5$ km s^{-1}, consistent with the b values of 3–5 km s^{-1} inferred for the $J'' = 2$–4 lines of H_2 from *Copernicus* observations (van Dishoeck & Black 1986, and references therein). The $J'' = 0$ and 1 lines lie on the square-root part of the curve of growth and are thus insensitive to small uncertainties in b (Savage et al. 1977).

[1] Based on the development and utilization of Orbiting and Retrievable Far and Extreme Ultraviolet Spectrometers (ORFEUS), a collaboration of the Astronomical Institute of the University of Tübingen, the Space Astrophysics Group of the University of California at Berkeley, and the Landessternwarte Heidelberg.

TABLE 1

TARGET SUMMARY

HD	l	b	Spectral Type	$E(B-V)$	d (pc)	$v \sin i$ (km s^{-1})	T (s)	S/N	References
41161	165.0	+12.9	O8 V	0.20	1253	300	814	45.2	1, 2
54911	229.0	−3.1	B1 III	0.14	1893	100:	2462	78.0	1, 3
93129a.....	287.4	−0.6	O3 If*	0.54	3470	120	3045	36.2	4, 5
94493	289.0	−1.2	B0.5 Iab/Ib	0.20	3327	145	1528	34.9	1, 3
99857	294.8	−4.9	B1 Ib	0.33	3058	180	1383	22.3	1, 3
99890	291.8	+4.4	B0.5 V:	0.24	3070	180	2532	39.7	1, 3
104705.....	297.5	−0.3	B0 III/IV	0.26	3898	215	1788	36.3	1, 3

REFERENCES.—(1) Fruscione et al. 1994; (2) rotational velocity from Jenkins 1978; (3) rotational velocity from Savage & Massa 1987; (4) Walborn 1973; (5) Gies 1987.

To provide an estimate of the stellar continuum, we make use of reference spectra selected from the 0.2 Å *Copernicus* Spectral Atlas (Snow & Jenkins 1977). Atlas counterparts, listed in Table 3, are selected for their similarity to the observed stars in MK classification, and, where possible, in $v \sin i$. The atlas spectra are smoothed to the resolution of the ORFEUS data, resampled at the ORFEUS pixel size, and scaled by a linear function to reproduce the observed stellar continuum. Because the total H_2 column density $N(H_2)$ in each reference spectrum is less than the uncertainty in either the $J'' = 0$ or $J'' = 1$ column of the corresponding program star, we do not attempt to correct for H_2 absorption in the reference spectrum. For HD 93129a, an O3 If* star, we expect the photospheric lines to be quite weak (Taresch et al. 1997) and therefore assume a linear continuum in modeling the interstellar absorption in its spectrum.

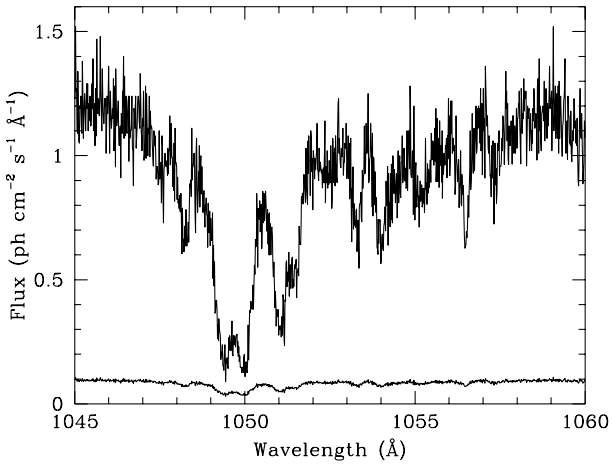

FIG. 1.—Portion of the ORFEUS spectrum of HD 99890. The spectrum has been background subtracted and flux calibrated and is plotted in photon units at full resolution. Principal absorption features are identified in Fig. 2. The error spectrum is also shown.

Following Hurwitz & Bowyer (1996), we adopt 0.31 Å as the FWHM of the instrument point-spread function. In the course of this work, we have discovered small nonlinearities in the ORFEUS wavelength calibration that will have to be quantified before the velocities of the absorbing clouds can be constrained. For this analysis, we assume that the clouds have zero radial velocity and adapt the wavelength scale accordingly.

To perform the model fit, we concentrate on the region between 1045 and 1060 Å, which contains most of the $v = 0 \rightarrow 4$ vibrational band in the Lyman series, as this region seems least complicated by stellar photospheric absorption or overlapping Werner bands of interstellar H_2. The process is iterative: we begin by fitting the $J'' = 0$ and $J'' = 1$ lines, move on to the higher J'' lines, then repeat the process, as the higher J'' lines often lie on the wings of lower J'' features. Isolated features elsewhere in the spectrum provide a double check on our results. The large number of free parameters and the computationally intensive nature of our fitting routine make an automated χ^2 reduction algorithm impractical. Instead, we vary the model column density about the best-fit value until the model line profile departs significantly from the data and use this as an estimate of the uncertainty in the fit. Column densities derived in this way for the $J'' = 0$–5 rotational levels of H_2 are

TABLE 2

MEASURED PARAMETERS OF INDIVIDUAL VELOCITY COMPONENTS

HD	Species	Component Number	$\langle v_i \rangle$ (km s^{-1})	b_i (km s^{-1})	N_i (cm^{-2})	Notes
54911	Na I	1	7.5 ± 0.1	3.0 ± 0.1	3.90 ± 0.18(12)	1
		2	18.3 ± 0.1	1.8 ± 0.1	1.71 ± 0.12(12)	
93129a.....	Ca II, Na I	1	−33	...	...	2
		2	0	...	...	
94493	Na I	1	17.7 ± 0.1	5.6 ± 0.1	5.52 ± 0.07(12)	1
		2	0.6 ± 0.1	4.0 ± 0.1	3.55 ± 0.07(12)	
104705.....	Na I	1	−30.7 ± 0.2	2.2 ± 0.2	1.69 ± 0.46(12)	1
		2	−22.2 ± 0.2	2.4 ± 0.2	1.23 ± 0.13(12)	
		3	0.3 ± 0.1	3.4 ± 0.1	5.27 ± 0.39(12)	

NOTES.—(1) Principal absorption components along lines of sight observed by Sembach et al. 1993; (2) Walborn 1982 find a number of weak interstellar features between −13 and +19 km s^{-1}, which we render as a single velocity component at 0 km s^{-1} with a column density twice that of the −33 km s^{-1} feature. We assume $b = 5$ km s^{-1} for both components.

TABLE 3

COPERNICUS[a] CONTINUUM REFERENCE STARS

Program Star HD	Atlas Star Name	Atlas Star HD	Spectral Type	$E(B-V)$	$v \sin i$ (km s^{-1})	log $N(H_2)$[b] (cm^{-2})
41161	15 Mon	47839	O7 V((f))	0.07	106	15.55
54911	β Cen A	122451	B1 III	0.02	70	12.8
93129a	None	...	...	...	...	...
94493	κ Ori	38771	B0.5 Ia	0.07	81	15.68
99857	κ Ori	...	...	...	...	...
99890	θ Car	93030	B0.5 Vp	0.06	130	<17.65
104705	κ Ori	...	...	...	...	...

[a] Snow & Jenkins 1977.
[b] Savage et al. 1977.

presented in Table 4. We estimate uncertainties of 0.2 dex for $J'' = 0$–3 and 0.5 dex for $J'' \geq 4$. Figure 2 presents the spectrum of HD 99890 between 1045 and 1060 Å, together with our best-fitting model.

To investigate the uncertainty introduced by assuming a single absorption component in the spectra of stars lacking published absorption-line parameters, we generate a series of synthetic spectra (with S/N $\sim$ 35), each with two absorption components of equal column density, separated by 5, 15, 25, 35, and 45 km s^{-1}, respectively. We fit a model to each synthetic spectrum, assuming a single velocity component. For the $J'' = 0$ and $J'' = 1$ states, the derived column densities differ by less than our quoted uncertainty over the entire 5–45 km s^{-1} range. For the $J'' = 2$ and $J'' = 3$ states, however, the difference can be significant—as great as 1.5 dex for the $J'' = 3$ state in the 25 and 35 km s^{-1} models, in the sense that a single-cloud model overestimates the total column density in the $J'' = 3$ state. The $J'' = 4$ and $J'' = 5$ states vary, but not by more than our estimated uncertainties (0.5 dex). Fortunately, the total column $N(H_2)$ is dominated by the $J'' = 0$ and $J'' = 1$ states (Spitzer, Cochran, & Hirschfeld 1974). The values of n and T_{01} derived in § 3 are thus insensitive to uncertainties in the velocity structure of the absorbing medium.

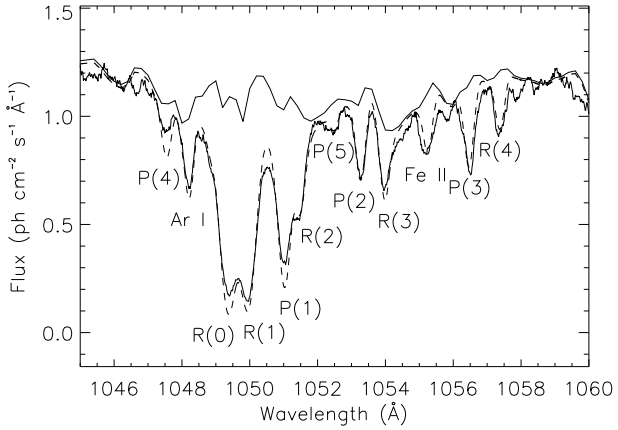

FIG. 2.—The $v = 0 \rightarrow 4$ vibrational band in the Lyman series of molecular hydrogen from the ORFEUS spectrum of HD 99890. The data have been smoothed with a 13 pixel boxcar. Overplotted are our best-fitting model (*dashed line*) and the spectrum of θ Car from the *Copernicus* Spectral Atlas (Snow & Jenkins 1977), which we use to model the stellar features in the HD 99890 spectrum.

3. ANALYSIS

The strongest UV lines arise from the $J'' = 0$ and $J'' = 1$ levels, whose relative populations are established by thermal proton collisions, since the molecules are protected from photoexcitation by self-shielding in the lines. The mean excitation temperature of the clouds along each line of sight can thus be derived from the column densities $N(0)$ and $N(1)$, using the relation

$$\frac{N(1)}{N(0)} = \frac{g_1}{g_0} \exp \frac{-E_{01}}{kT_{01}} = 9 \exp \frac{-170 \text{ K}}{T_{01}}, \quad (1)$$

where g_0 and g_1 are the statistical weights of $J'' = 0$ and $J'' = 1$, respectively (Shull & Beckwith 1982). Cloud temperatures for the ORFEUS lines of sight are presented in

TABLE 4

COLUMN DENSITIES

HD	N(H I)[a]	$N(H_2)$	$N(0)$	$N(1)$	$N(2)$	$N(3)$	$N(4)$	$N(5)$	$N(4)/N(0)$[b]	T_{01}[c] (K)	n[d] (cm^{-3})
41161	21.01	20.0	19.7	19.7	17.6	17.6	15.0	14.2	−4.7	77	16
54911	21.13	19.6	19.3	19.3	17.4	16.9	14.5	13.9	−4.8	77	8
93129a.....	21.40	20.1	19.7	19.9	17.2	16.9	15.9	16.1	−3.8	98	6
94493	21.11	20.1	19.7	19.8	17.7	16.2	15.0	15.1	−4.7	86	13
99857	21.31	20.2	19.8	20.0	18.5	18.2	16.2	15.4	−3.6	97	9
99890	20.93	19.6	19.2	19.3	17.7	17.6	16.0	14.7	−3.2	86	11
104705.....	21.11	20.0	19.7	19.7	17.5	16.6	14.6	...	−5.1	77	13

NOTE.—All column densities are given as logarithms. Units are cm^{-2}. Estimated uncertainties are 0.2 dex for $J'' = 0$–3 and 0.5 dex for $J'' \geq 4$.

[a] H I column densities from the compilation of Fruscione et al. 1994, except for HD 93129a, which is from Taresch et al. 1997.
[b] log $[N(4)/N(0)]$. Values greater than −4.8 may indicate the presence of a radiation field several times that in the solar neighborhood. Uncertainties in this ratio are $\sim$0.5 dex. See § 3.
[c] Cloud temperature derived from $N(1)/N(0)$. Uncertainties are $\sim$33%. See § 3.
[d] Lower limit to cloud proton (H I + 2H_2) density derived from N(H I), $N(H_2)$, and T_{01}. See § 3.

Table 4. Our results are consistent with those obtained with *Copernicus* by Savage et al. (1977), who derive values of T_{01} ranging from 45 to 128 K, with an average of 77 ± 17 (rms) K, for 61 stars with $N(H_2) > 10^{18}$ cm^{-2}.

We estimate the cloud density n using the relation derived by Reach, Koo, & Heiles (1994),

$$\left(\frac{n}{50\ \mathrm{cm}^{-3}}\right)^2 \simeq \frac{N(H_2)}{10^{19}\ \mathrm{cm}^{-2}}\left(\frac{T}{80\ \mathrm{K}}\right)^{-1}\left[\frac{N(\mathrm{H\ I})}{10^{20}\ \mathrm{cm}^{-2}}\right]^{-2}, \quad (2)$$

where n is the proton (H I + $2H_2$) volume density and the values of N(H I), $N(H_2)$, and T_{01} are from Table 4. The resulting cloud densities, presented in Table 4, are lower limits for two reasons: first, because an unknown fraction of N(H I) lies outside of the H_2-bearing clouds, and second, because the relation assumes a single cloud along the line of sight. If the observed H I and H_2 columns were divided evenly among n_c clouds, for example, the density of each cloud would rise as $(n_c)^{1/2}$. The density limits derived via equation (2) are consistent with the values between 15 and 900 cm^{-3} found by Jura (1975) for interstellar clouds containing optically thick H_2.

While detailed modeling of the relative J'' column densities is beyond the scope of this paper, we can investigate the radiation environments of the H_2 clouds by comparing our observations with the predictions of previously published models. Jura (1975) models the $J'' = 0$–6 column densities along 10 lines of sight observed with *Copernicus*. He finds that the ratios $N(4)/N(0)$ and $N(5)/N(1)$ are controlled by the optical pumping rate, rather than by the electron temperature of the cloud, and concludes that clouds along four lines of sight are illuminated by an ultraviolet field several times greater than that of the solar neighborhood. All four of these sight lines show values of $\log [N(4)/N(0)] > -4.8$. (A fifth sight line that also shows a high value of $N(4)/N(0)$ can be fitted without recourse to an elevated radiation field.) In Table 4, we see that five of our seven stars have $\log [N(4)/N(0)] > -4.8$. Given that the uncertainty in this ratio is ~0.5 dex, we consider only the three stars with the highest values of $N(4)/N(0)$: HD 93129a, HD 99857, and HD 99890. While his models assume a single absorbing cloud, Jura (1975) points out that if there are several clouds along the line of sight, the ultraviolet opacity within each cloud is lower than if only one cloud is present, and the observations can often be fitted with several clouds at normal UV levels, rather than with a single cloud with elevated illumination. Multiple-cloud models may be able to reproduce the high $N(4)/N(0)$ ratios that we observe. On the other hand, the absorbing clouds may simply lie near the hot background stars. For HD 93129a in the Carina Nebula, this is certainly the case (cf. Walborn, Heckathorn, & Hesser 1984).

4. DISCUSSION

Figures 3, 4, and 5, based on Figures 4–6 of Savage et al. (1977), explore the relationships among the H_2 column density $N(H_2)$, the fraction of hydrogen in the molecular state $f = 2N(H_2)/[N(\mathrm{H\ I}) + 2N(H_2)]$, the reddening $E(B-V)$, and the total hydrogen column density N(H I + H_2) = N(H I) + $2N(H_2)$. (Many of the *Copernicus* data points in the lower left of each diagram are actually upper limits.) Savage et al. (1977) found that lines of sight with low extinction [$E(B-V) \lesssim 0.08$] show low columns of H_2 and

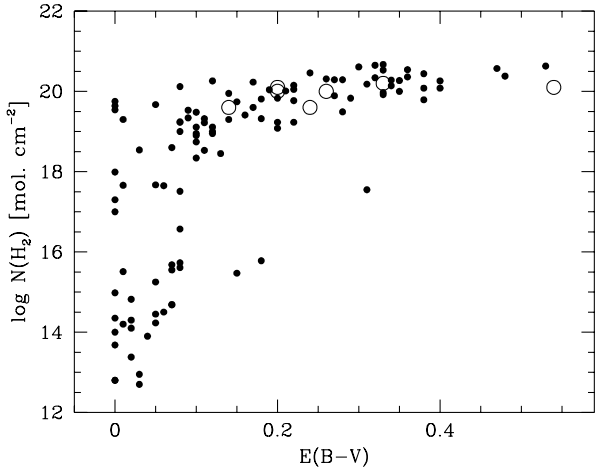

FIG. 3.—Logarithm of the total H_2 column density vs. $E(B-V)$, a measure of the dust column density. Solid symbols represent lines of sight observed with *Copernicus* (Savage et al. 1977). Many of the *Copernicus* points with $E(B-V) < 0.1$ are upper limits. Open symbols represent the seven stars observed with ORFEUS.

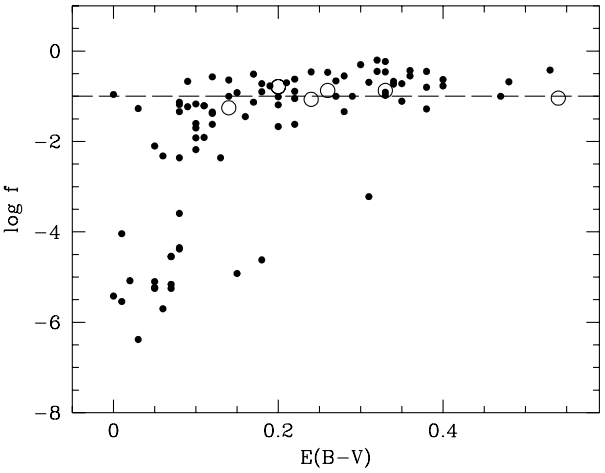

FIG. 4.—Logarithm of f, the fractional abundance of H_2, vs. $E(B-V)$. A dashed line marks the level at which $\log f = -1.0$. Solid symbols represent *Copernicus* observations, while the open symbols represent this work. Two ORFEUS data points with $E(B-V) = 0.20$ overlap.

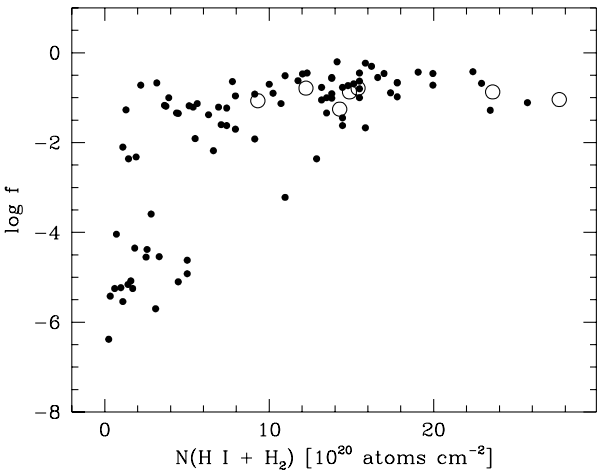

FIG. 5.—Plot of $\log f$ vs. the total hydrogen column density, N(H I + H_2) = N(H I) + $2N(H_2)$. Solid symbols represent *Copernicus* observations, while the open symbols are from this work.

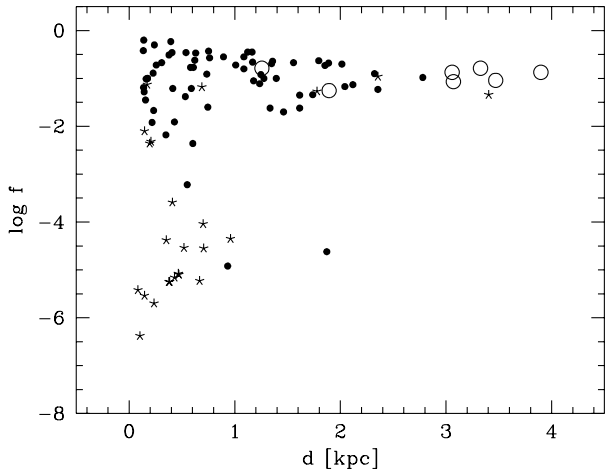

FIG. 6.—Plot of log f vs. the derived stellar distance. Solid symbols represent *Copernicus* observations, except for stars with $E(B-V) \leq 0.08$, which are plotted here as asterisks. The open symbols are from this work. We find that f remains $\sim 10\%$ even at large distances in the disk.

low values of f (~ 0.02), while those with higher extinction [$E(B-V) > 0.08$] show much higher H_2 columns and values of f that rise slowly with $E(B-V)$. The change from small to large f at $E(B-V) \approx 0.08$ and $N(\text{H I} + H_2) \approx 5 \times 10^{20}$ cm^{-2} is thought to reflect the column density at which the diffuse H_2-bearing clouds provide self-shielding against radiative dissociation.

The seven ORFEUS disk stars fall squarely in the "large-f" region of all three figures, indicating a common mechanism for H_2 production. We have seen that the cloud temperatures and density limits derived from the ORFEUS observations are consistent with those obtained with *Copernicus*. From the H_2 column densities $N(\text{H}) = 1\text{–}3 \times 10^{21}$ cm^{-2} and proton densities $n \sim 10$ cm^{-3} in Table 4, we estimate path lengths on the order of tens of parsecs, consistent with standard models (Wilson & Walmsley 1989).

The five stars in our sample with $d > 3$ kpc all lie at Galactic longitudes between 287° and 298°, providing lines of sight directly through the Sagittarius spiral arm. (The distances, taken from the literature, were originally derived from stellar spectral types and can be assumed to be accurate to about 25%; see Sembach, Danks, & Savage 1993.) Unless the Sagittarius arm is devoid of molecular gas, our results suggest that its clouds do not differ significantly in their gross properties from those near the Sun.

Savage et al. (1977) point out that *Copernicus* sampled lines of sight with relatively low reddening. While the mean reddening [$\Sigma E(B-V)/\Sigma r$] in the Galactic plane within 1 kpc of the Sun is 0.61 mag kpc^{-1} (Spitzer 1968), the mean reddening to the *Copernicus* stars is 0.22 mag kpc^{-1}. The mean reddening to the ORFEUS disk stars is even lower: 0.11 mag kpc^{-1}.

In Figure 6 we plot log f versus stellar distance. To highlight the different behaviors along high- and low-reddening lines of sight, stars with $E(B-V) \leq 0.08$ are plotted as asterisks. Savage et al. (1977) find a slow increase in f with $E(B-V)$ for $E(B-V) > 0.15$, a trend confirmed in our data (Fig. 4). As a function of distance, however, we see that f remains nearly flat out to 4 kpc. Because our sight lines do not sample Galactic radii very different from that of the Sun, we do not expect f to approach unity at large distances, as it does toward the inner Galaxy (Dame 1993). Nevertheless, it is remarkable that the molecular fraction of hydrogen should vary so little over the wide range of distances and mean densities sampled by *Copernicus* and ORFEUS. If the neutral and molecular hydrogen were not coupled, one might expect significant variations in the molecular fraction of hydrogen. On the other hand, a constant value of f is predicted by models in which most of the neutral ISM is associated with the H_2-bearing clouds, perhaps in a shell surrounding the molecular core (see McKee & Ostriker 1977).

Sembach & Danks (1994) find that the Na I and Ca II absorption profiles along low-density sight lines, including those to HD 54911, HD 94493, and HD 104705 (Table 2), show considerable structure from diffuse clouds. The number of components in the profiles is loosely correlated with n_0(H I), the average density of H I in the Galactic disk derived for a given line of sight, again suggestive of a patchy distribution for the neutral ISM along low-density lines of sight (Sembach & Danks 1994).

5. CONCLUSIONS

We have measured column densities for the $J'' = 0\text{–}5$ rotational states of H_2 in the spectra of seven disk stars ($z < 300$ pc) observed with the Berkeley EUV/FUV spectrometer on the ORFEUS telescope. These stars lie at distances of up to 3.9 kpc, allowing us to probe lines of sight much deeper into the Galactic disk than were heretofore available. Five of our sight lines intersect the Sagittarius spiral arm. Our data continue the relationship between H_2 column density and reddening established for the *Copernicus* clouds, indicating a common mechanism for H_2 production. Estimates of cloud temperatures and densities are consistent with those derived from *Copernicus* observations. The molecular fraction f is nearly constant over a wide range of distances and mean reddenings, consistent with a model in which the neutral component of the ISM is associated mainly with the H_2-bearing clouds.

This research has made use of the NASA ADS Abstract Service and the Catalogue Service of the CDS, Strasbourg, France. We thank J. Black for providing H_2 transition data in electronic format and C. McKee for helpful comments on the text. We acknowledge our colleagues on the ORFEUS team and the many NASA and DARA personnel who helped make the ORFEUS-I mission successful. This work is supported by NASA grant NAG5-696.

REFERENCES

Dame, T. M. 1993, in AIP Conf. Proc. 278, Back to the Galaxy, ed. S. S. Holt & F. Verter (New York: AIP), 267
Fruscione, A., Hawkins, I., Jelinsky, P., & Wiercigroch, A. 1994, ApJS, 94, 127
Gies, D. R. 1987, ApJS, 64, 545
Grewing, M., et al. 1991, in Extreme Ultraviolet Astronomy, ed. R. F. Malina & S. Bowyer (New York: Pergamon), 437
Hurwitz, M., & Bowyer, S. 1991, in Extreme Ultraviolet Astronomy, ed. R. F. Malina & S. Bowyer (New York: Pergamon), 442
———. 1995, ApJ, 446, 812
———. 1996, ApJ, 465, 296
Hurwitz, M., Bowyer, S., Kudritzki, R.-P., & Lennon, D. J. 1995, ApJ, 450, 149
Jenkins, E. B. 1978, ApJ, 219, 845

Jura, M. 1975, ApJ, 197, 581
McKee, C. F., & Ostriker, J. P. 1977, ApJ, 218, 148
Reach, W. T., Koo, B.-C., & Heiles, C. 1994, ApJ, 429, 672
Savage, B. D., Bohlin, R. C., Drake, J. F., & Budich, W. 1977, ApJ, 216, 291
Savage, B. D., & Massa, D. 1987, ApJ, 314, 380
Sembach, K. R., & Danks, A. C. 1994, A&A, 289, 539
Sembach, K. R., Danks, A. C., & Savage, B. D. 1993, A&AS, 100, 107
Shull, J. M., & Beckwith, S. 1982, ARA&A, 20, 163
Snow, T. P., Jr., & Jenkins, E. B. 1977, ApJS, 33, 269
Spitzer, L. 1968, Diffuse Matter in Space (New York: Interscience), 67
Spitzer, L., Cochran, W. D., & Hirschfeld, A. 1974, ApJS, 28, 373
Taresch, G., et al. 1997, A&A, 321, 531
van Dishoeck, E. F., & Black, J. H. 1986, ApJS, 62, 109
Vennes, S., & Fontaine, G. 1992, ApJ, 401, 288
Walborn, N. R. 1973, ApJ, 179, 517
———. 1982, ApJS, 48, 145
Walborn, N. R., Heckathorn, J. N., & Hesser, J. E. 1984, ApJ, 276, 524
Wilson, T. L., & Walmsley, C. M. 1989, A&A Rev., 1, 141